

ORIGINAL ARTICLE

Chemolithotrophic processes in the bacterial communities on the surface of mineral-enriched biochars

Jun Ye^{1,2}, Stephen D Joseph^{3,4}, Mukan Ji², Shaun Nielsen¹, David RG Mitchell⁵, Scott Donne⁶, Joseph Horvat⁷, Jianli Wang⁷, Paul Munroe³ and Torsten Thomas^{1,8}

¹Centre for Marine Bio-Innovation, The University of New South Wales, Sydney, New South Wales, Australia; ²School of Biotechnology and Biomolecular Sciences, The University of New South Wales, Sydney, New South Wales, Australia; ³School of Materials Science and Engineering, The University of New South Wales, Sydney, New South Wales, Australia; ⁴Institute of Resource, Ecosystem and Environment of Agriculture, Nanjing Agricultural University, Nanjing, China; ⁵Australian Institute of Innovative Materials, University of Wollongong, Wollongong, New South Wales, Australia; ⁶School of Environmental and Life Sciences, University of Newcastle, Newcastle, New South Wales, Australia; ⁷Institute for Superconducting and Electronic Materials, University of Wollongong, Wollongong, New South Wales, Australia and ⁸School of Biological, Earth and Environmental Sciences, The University of New South Wales, Sydney, New South Wales, Australia

Biochar and mineral-enriched biochar (MEB) have been used as soil amendments to improve soil fertility, sequester carbon and mitigate greenhouse gas emissions. Such beneficial outcomes could be partially mediated by soil bacteria, however little is known about how they directly interact with biochar or MEB. We therefore analyzed the diversity and functions of bacterial communities on the surfaces of one biochar and two different MEBs after a 140-day incubation in soil. The results show that the biochar and the MEBs harbor distinct bacterial communities to the bulk soil. Communities on biochar and MEBs were dominated by a novel Gammaproteobacterium. Genome reconstruction combined with electron microscopy and high-resolution elemental analysis revealed that the bacterium generates energy from the oxidation of iron that is present on the surface. Two other bacteria belonging to the genus *Thiobacillus* and a novel group within the *Oxalbacteraceae* were enriched only on the MEBs and they had the genetic capacity for thiosulfate oxidation. All three surface-enriched bacteria also had the capacity to fix carbon dioxide, either in a potentially strictly autotrophic or mixotrophic manner. Our results show the dominance of chemolithotrophic processes on the surface of biochar and MEB that can contribute to carbon sequestration in soil.

The ISME Journal (2017) 11, 1087–1101; doi:10.1038/ismej.2016.187; published online 7 February 2017

Introduction

Biochar is a carbon-rich solid material derived from the thermal processing of biomass in an oxygen-depleted environment (Lehmann and Joseph, 2015). The application of biochar to soil has shown promising results for the sequestration of carbon (Lehmann *et al.*, 2006), the mitigation of greenhouse gas emissions (Woolf *et al.*, 2010), the immobilization of heavy metals (Cao *et al.*, 2011) and the improvement of soil fertility (Kolton *et al.*, 2011).

However, biochars often have to be applied in high rates (10–100 t ha⁻¹) to agricultural soils to deliver such positive outcomes (Jeffery *et al.*, 2011). Recent findings have shown that biochar naturally forms aggregates with minerals in the highly fertile Amazonian Dark Earths (Chia *et al.*, 2012). This has led to the manufacturing of biochars with coatings of ground rocks, clays and other minerals to form so called mineral-enriched biochar (MEB; Chia *et al.*, 2014). At low application rates (~5 t ha⁻¹) these MEBs have been found to produce sweet corn yields comparable to traditional fertilizer (Nielsen *et al.*, 2014) and improve productivity of pakchoi in organic farming (Ye *et al.*, 2016).

The beneficial effects of biochar or MEB have been attributed to their recalcitrance, conductivity, porosity and adsorption properties, which depend on the biomass feedstock, pyrolysis conditions and mineral

Correspondence: T Thomas, Centre of Marine Bio-Innovation and School of Biological, Earth and Environmental Sciences, University of New South Wales, High Street, Sydney, New South Wales 2052, Australia.

E-mail: t.thomas@unsw.edu.au

Received 28 June 2016; revised 17 September 2016; accepted 9 December 2016; published online 7 February 2017

additives, if used (Chia *et al.*, 2015). However, biochar and MEB have also been shown to cause shifts in microbial communities (O'Neill *et al.*, 2009; Anderson *et al.*, 2011; Nielsen *et al.*, 2014; Abujabhah *et al.*, 2016) and this might indirectly impact biogeochemical processes in soil (Lehmann *et al.*, 2011; Bardgett and van der Putten, 2014). For example, a corn stalk biochar has been shown to increase the abundances of methanotrophic proteobacteria in a Chinese paddy soil (Feng *et al.*, 2012), a jarrah wood MEB increased soil nitrifiers (Ye *et al.*, 2016) and a green waste biochar stimulated N₂O-reducing bacteria (Harter *et al.*, 2014). These and other studies have mainly focused on bulk measurements of amended soils to explain the microbial processes behind the beneficial effects of biochar and MEB, while very few studies have examined the specific interactions between the biochar surfaces and microorganisms.

It has been well recognized that soil microorganisms colonize surfaces of soil particles, which provide specific habitats in terms of inorganic and organic substrates, oxygen level or redox conditions (Sessitsch *et al.*, 2001; Mills, 2003). Different soil particle fractions often harbor different microbial communities and hence support distinct metabolic processes (Hemkemeyer *et al.*, 2015). Likewise, biochar has been suggested to provide habitats for microorganisms when added to soils (Pietikäinen *et al.*, 2000; Lehmann *et al.*, 2011; Quilliam *et al.*, 2013). Indeed, Sun *et al.* (2016) recently reported for the first time that bacterial communities on biochar particles and bulk soil do significantly differ. In addition, the study used 16S rRNA gene sequence analysis and a Phylogenetic Investigation of Communities by Reconstruction of Unobserved States (PICRUSt; Langille *et al.*, 2013) to predict that the bacterial communities on biochar particles prefer to metabolize xenobiotics. However, given that soil microorganisms are highly diverse and largely uncharacterized (Rondon *et al.*, 1999; Fierer and Jackson, 2006), it is likely that certain metabolic traits of bacterial communities on biochar surface have been missed by such purely 16S rRNA-based functional predictions.

To improve our understanding of the processes that occur on biochar surfaces, we investigate here bacterial communities and their functions on a bamboo biochar and two biochars enriched with minerals. We hypothesized that specific bacterial communities would be recruited by the different biochars and that they carry out distinct functions that are determined by specific aspects of the biochar surface. Using amplicon sequencing of the bacterial 16S rRNA gene and metagenomics, we show a substantial surface enrichment of specific soil bacteria that have the capacity for different kinds of chemolithotrophy based on genome-based predictions. We then use a novel gold-label *in situ* hybridization (GISH) method (Ye *et al.*, 2015) and scanning electron microscopy to localize a dominant bacterium on the biochar particles. Using scanning

transmission electron microscopy (STEM), energy-dispersive X-ray spectroscopy (EDS) and electron energy loss spectroscopy (EELS) we show that this dominant bacterium is involved in iron oxidation, which could support CO₂ fixation on the biochar surface.

Materials and methods

Study soil, biochar production and analysis

Red chromosol soils (Australia Soil Classification) used in this study came from a farmland site located in Dubbo, central NSW, Australia (32°13'S, 148°59'E). The farmland is within a temperate climate zone with a mean annual rainfall of 584.4 mm and a mean annual temperature of 17.3 °C. The plough layer (0–20 cm in depth) was collected after crop harvest, homogenized and sieved through a 2 mm mesh.

Three different biochars were made from a single length of bamboo to minimize natural variation in organic chemistry and mineral content. Two of these biochars were treated with minerals and clays to produce MEBs. For this, bamboo was cut into cubes (dimension of 1 cm), which were randomly divided into three equal parts. Two types of mineral slurries were prepared by dissolving either refined bentonite clay or kaolinite clay (Keane Ceramics, Somersby, Australia) with ferrous sulfate heptahydrate (FeSO₄·7H₂O, Sigma-Aldrich, Castle Hill, NSW, Australia) in water at a ratio of 1:1:20 (w/w/w). Bentonite is a smectite with a different crystal structure and chemical properties to kaolinite, especially in relation to reaction with organic matter (Yariv and Cross, 2001). Our recent study has demonstrated that addition of bentonite produces a biochar with significantly different carbon structure to that with kaolinite (Rawal *et al.*, 2016). Biochars produced from biomass that has been enriched with iron salts and clays are also generally much more redox active, store significant quantities of charge under oxygen-starved conditions and have different magnetic properties compared to biochars made from virgin biomass (Joseph *et al.*, 2015). Two batches of the bamboo cubes were treated by soaking in either of the two slurries at 80 °C for 3 h. These two slurry-treated batches and the untreated batch were dried at 110 °C for 24 h. Bamboo cubes were then placed into a lab-scale pyrolysis reactor and heated in an oxygen-free environment with a heating rate of 3 °C min⁻¹ to reach 450 °C and kept there for 30 min. The material was then cooled down and stored under sterile condition until use. These three products were referred to as bamboo biochar (Bam), bentonite biochar (Ben) and kaolinite biochar (Kao).

The chemical compositions of each type of biochar were determined using a vario EL III elemental analyzer (Elementar, Langenselbold, Germany). The dissolved organic carbon and total soluble nitrogen were extracted with 25 ml of 0.5 M potassium sulfate in an orbital shaker for 1 h at 250 r.p.m. The extracts were then analyzed

Table 1 Composition of the biochar used in this study

	<i>Bam</i>	<i>Ben</i>	<i>Kao</i>
Yield %	35	42	48
C %	75	61	62.9
H %	3.42	2.79	2.82
N %	1.38	0.84	1.45
S %	0.12	1.3	1.1
Fe %	0.023	2.5	2.9
Ca %	0.098	0.12	0.069
Al %	0.0051	0.034	0.093
K %	1.4	0.63	1.2
Ash %	19.1	56.87	35.6
DOC mg g ⁻¹ C	1.45	8.26	8.04
TSN mg g ⁻¹ N	ND	0.13	0.5

Abbreviations: Bam, bamboo biochar; Ben, bentonite biochar; DOC, dissolved organic carbon; DON, dissolved organic nitrogen; Kao, kaolinite biochar; ND, not detected; TSN, total soluble nitrogen. Yield was calculated as the weight of dry biochar (after pyrolysis) as proportion of the dry feedstock weight (before pyrolysis). Note that the ash content also includes individual elements that are listed.

using a TOC/TN_b analyzer (Analytik Jena, Überlingen, Germany). Results are summarized in Table 1.

Experimental design and set-up

Just before application to the soil, the biochar and MEBs were milled into small pieces (1–5 mm) using sterile mortars and pestles. The biochar and MEBs were applied to soil at a rate of 0.5% w/w (equivalent to 6.5 t ha⁻¹ to a 10 cm soil profile). Mono-ammonium phosphate was either not added or at a rate of 0.1% w/w (equivalent to 130 kg ha⁻¹ N and 284.7 kg ha⁻¹ P to a 10 cm soil profile) to represent ‘real-world’ agricultural applications of biochar, which can occur with or without additional fertilization (Nielsen *et al.*, 2014). This crossed design, including controls, resulted in eight treatments: no biochar, Bam, Ben or Kao, each with or without mono-ammonium phosphate. Two hundred grams of soil were mixed with the corresponding amounts of milled biochar/MEBs and/or fertilizer on a sterile working bench before being placed into pots (top side 5 cm, bottom side 4 cm and height 12 cm). Triplicate pots for each of the eight treatments were randomly arranged in a 6 × 4 array on a bench within the greenhouse facility of the University of New South Wales (UNSW). The water content was maintained at 50% water holding capacity during the incubation.

The incubation was stopped after 140 days. This incubation period was chosen to reflect a reasonable approximate of a crop cycle (4–5 months) and because the mean residence time of the labile carbon pool of biochar was found to be about 108 days (Wang *et al.*, 2016). This latter fact means that microbial processes on the biochar and MEB will likely not anymore be influenced by variable leaching of carbon from the biochar. To process samples after incubation, the content of each pot was poured into individual sterile petri dishes. Biochar particles were manually picked out with sterile forceps. An aliquot of soil without biochar particles was also taken from this. Biochar particles were transferred onto a sterile 1 mm metal

mesh and washed with sterile deionized water to remove attached soil. Soil and biochar particles were stored at –80 °C until further use.

Bacterial 16S rRNA gene analysis

Total DNA was extracted from soil and biochar particles using the PowerSoil DNA isolation kit (MO BIO Laboratories, Carlsbad, CA, USA) according to the manufacturer’s instruction, but with minor modification for biochar particles. The kit has a loading capacity of 0.25 g for soil, but the biochar particles have a low density and hence an equivalent weight could not fit into the tube. Therefore 0.1 g of biochar particles were used, which gave sufficient DNA yields for subsequent analysis. Extracted DNA was checked for quality and quantity using agarose gel electrophoresis and a Qubit fluorometer (Invitrogen, Carlsbad, CA, USA).

The V1–V3 regions of the 16S rRNA gene were amplified using the primers 27F (5′-AGAGTTTGAT CMTGGCTCAG-3′) and 519R (5′-GWATTACCGCGG CKGCTG-3′) that target conserved sequences found in bacteria. Amplicons from each PCR sample were normalized to equimolar amounts and sequenced using 2 × 300 bp chemistry on a MiSeq platform (Illumina, San Diego, CA, USA) at the Ramaciotti Centre for Genomics (UNSW). 16S rRNA sequencing data was processed using the MOTHUR MiSeq pipeline (Kozich *et al.*, 2013) and details are provided in the Supplementary Information. In total 2 180 232 high-quality 16S rRNA sequences were generated for 36 samples. After subsampling each sample to an equal sequencing depth (60 562 reads per sample) and clustering, 14 244 operational taxonomic units (OTUs) at 97% identity were obtained, with the number of OTUs ranging from 1193 to 3988 per sample. The Good’s coverage for the observed OTUs was 99.46 ± 0.02% (mean ± s.e.m.) and the rarefaction curves showed clear asymptotes (Supplementary Figure 1), which together indicate a near-complete sampling of the community.

Statistical analysis

The experimental design consisted of three factors, including biochar type (no biochar, Bam, Ben and Kao), fertilizer (F, NF) and sample type (soil, particle). The bacterial β-diversity was compared using the Bray–Curtis similarity coefficient calculated on square-root transformed, relative abundances of OTUs and the resulting dissimilarity matrix was mapped using non-metric multidimensional scaling in the vegan package of R (Oksanen *et al.*, 2015). Permutational analysis of variance (PERMANOVA, using 10⁴ permutations) was applied to the Bray–Curtis dissimilarity matrix to test the significance levels of differences for each experimental factor using PRIMER V6 (Anderson *et al.*, 2008). The Welch’s t-test within STAMP (Parks *et al.*, 2014) was used to identify OTUs that showed significant differences in abundance between groups (confidence interval method). Unless otherwise indicated, *P*-values

were adjusted for multiple comparisons using the Storey false discovery rate and displayed as *q*-value (Krzywinski and Altman, 2014).

Metagenomic sequencing and assembly

After checking for quality and quantity of community DNA extracted from biochar particles, three samples from the treatments of Ben-F-particle, Kao-NF-particle and Kao-F-particle had sufficient high-quality DNA suitable for metagenomic sequencing. Sequencing libraries for these samples were generated with the NexteraXT kit following the manufacturer's instructions (Illumina). The libraries were sequenced with an Illumina NextSeq 500 sequencer using 150-bp paired-end reads at the Australian Centre for Ecogenomics (The University of Queensland, Australia). Approximately 66.5 million read pairs were generated on average per sample after filtering by PRINSEQ (Schmieder and Edwards, 2011). The metagenomic reads for each sample were assembled into contigs using IDBA-UD with iterative *k*-values setting from 80 to 100 (Peng *et al.*, 2012). All contigs were submitted to the Integrated Microbial Genomes/Expert Review (IMG/ER) system for gene calling and annotation (Markowitz *et al.*, 2012).

Binning and annotation of draft genomes

Sequencing reads of all three samples were mapped to contigs longer than 1 kb using Bowtie2 (Langmead and Salzberg, 2012). These contigs were then grouped into genome bins on the basis of coverage and tetranucleotide frequency using MetaBat (Kang *et al.*, 2015) with the 'very specific' option to minimize contaminations. Completeness and contamination of genome bins were assessed using CheckM (Parks *et al.*, 2015). The genome completeness was estimated by calculating the number of conserved single-copy marker genes recovered from individual genomic bins. Genome contamination was evaluated from the number of multi-copy marker genes. Genome bins that were greater than 80% completed and with less than 4% contamination were considered in this study, which resulted in 11 genome bins. Phylosift were used to evaluate taxonomy of each genome bin (Darling *et al.*, 2014). All genome bins were submitted to the IMG/ER for annotation and gene calling.

Phylogenetic analysis for OTU0001 and OTU0017

The representative sequences of the Gammaproteobacterium OTU0001 and *Oxalobacteraceae* OTU0017 were extracted from the amplicon sequence data. Separately for each OTU, we retrieved 16S rRNA gene sequences (>1300 nt) of the top 50 most closely related type strains from the nucleotide (nt) database at the National Center for Biotechnology Information (NCBI) using BLASTN (Morgulis *et al.*, 2008) and aligned those with the corresponding OTU sequence

using the SINA web aligner (Pruesse *et al.*, 2012). A phylogenetic tree was constructed using the neighbor joining algorithm in the ARB software package with Jukes-Cantor distance correction (Westram *et al.*, 2011) and its robustness was tested with 1000 bootstraps. We also retrieved 16S rRNA gene sequences of uncultured organisms that very closely related to OTU0001/OTU0017 via BLASTN from the nt database. Only sequences with explicit descriptions of their sources were retained and these were inserted into the phylogenetic tree using the parsimony insertion method (Westram *et al.*, 2011).

Classification of RuBisCo proteins

The genomes of the three bacteria dominating the surface community of biochar contained genes encoding for the ribulose-1,5-bisphosphate carboxylase/oxygenase (RuBisCO) and these were further investigated here. Functionally validated reference sequences were obtained from the scientific literature to determine the phylogeny of the RuBisCO large subunit genes (*rbcL*). Form II, III and IV RbcL sequences were obtained from Tabita *et al.* (2008), while form IA, IBc and IC RbcL sequences were from Badger and Bek (2008). The extracted RbcL sequences from the genome bins were aligned against those reference sequences using ClustalX (Larkin *et al.*, 2007), and then manually curated using Mega (Kumar *et al.*, 2008). A maximum likelihood phylogenetic tree was constructed using FastTree with a generalized time-reversible model (Price *et al.*, 2010). The confidence level of the tree topology was evaluated by bootstrap analysis using 1000 sequence replications.

Nucleotide accession numbers

All raw sequencing data sets of this study have been deposited in NCBI Sequence Read Archive. Amplicon sequences of the 16S rRNA genes were deposited in NCBI BioProject PRJNA313136. The shotgun sequences are available through accession numbers SRR3569623, SRR3569832 and SRR3569833 under PRJNA313136. The annotations of assembled contigs are accessible under the IMG Genome ID 3300005260, 3300005258, 3300005238. The genomic bins of Gama1 (*Gammaproteobacterium*), Oxal1 (*Oxalobacteraceae*) and Thio1 (*Thiobacillus*) are accessible under the IMG Genome ID 2627853547, 2627853544 and 2627853545, respectively.

Localization of OTU0001 on biochar particles

OTU0001 was detected using GISH. Briefly, biochar particles were washed in phosphate buffered saline (PBS, 20 mM NaH₂PO₄, 150 mM NaCl, 1 mM EDTA, pH 6.5) and fixed in 4% (v/v) paraformaldehyde at 4 °C for 24 h. Fixed biochar particles were then washed in PBS and stored in 1:1 mixture of PBS and absolute ethanol at -20 °C. A nanogold-labeled

probe specific for OTU0001 (see Supplementary Information) was hybridized with the fixed biochar particles. Biochar particles were dehydrated and coated with an evaporated carbon layer (JEE-420 Evaporative Carbon Coater, JEOL, Peabody, MA, USA). Images of secondary electrons and backscattered electrons were generated with a JEOL 7001F field emission scanning electron microscopy (JEOL, Freising, Germany). Elemental analyses were conducted using a JEOL silicon drift EDS. Details are provided in the Supplementary Information.

Compositional and oxidation state analysis of particles in contact with OTU0001

A GISH-treated biochar particle was first lightly ground into small pieces in absolute ethanol and then transferred onto a lacey carbon support film on a copper grid inside a JEM-ARM200F aberration-corrected STEM (JEOL, Japan). After the specimen was air dried, initial imaging in bright-field and high-angle annular dark-field (HAADF) were acquired at 200 kV accelerating voltage in a scanning mode using a 5C (0.155 nA) probe and a 40 μm condenser aperture. A NORAN system 7 X-ray Microanalysis System (Thermo Fisher, Fremont, CA, USA) coupled with a large area (1 steradian) JEOL EDS detector was used for compositional spectral imaging (SI) mapping and a GIF Quantum Energy Filter (Gatan, Warrendale, PA, USA) was used for oxidation state analyses based on an EELS.

Results and discussions

Enrichment of bacteria on the surface of biochar

The factors of biochar type, fertilizer and sample type significantly influenced bacterial β-diversity as

shown in a non-metric multidimensional scaling plot (Figure 1a). PERMANOVA detected significant effects associated with the interactions between biochar type and fertilizer ($P=0.03$), as well as fertilizer and sample type ($P=0.04$). There were neither significant interactions between biochar type and sample type ($P=0.34$), nor among these three factors ($P=0.66$; Supplementary Table 1). Together these results show that (i) biochar at a 6.5 t ha^{-1} application rate, with or without fertilizers, had no impact on the bacterial community composition of bulk soil over a 140 days incubation, (ii) the addition of fertilizer had a significant impact on bacterial communities in soil and the biochar particle, (iii) the bacterial communities on the biochar particles were significantly different from those in bulk soils irrespective if fertilizer was present or not and (iv) the bacterial communities on the two types of MEB particles were significantly different from Bam particles when no fertilizers were applied, however this distinction was disrupted when fertilizer was present.

We then investigated the bacterial taxa that accounted for the observed differences between biochar particles and bulk soils (Figure 1a). Independent of the variation caused by fertilizer application and biochar type, there were several bacterial taxa that accounted for these differences. In particular three OTUs were dominating the communities found on biochar particles and were in very low abundance in bulk soils (Figure 1b). These three OTUs could be taxonomically assigned to the class Gammaproteobacteria (OTU0001), the family *Oxalobacteraceae* (OTU0017) and the genus *Thiobacillus* (OTU0123). Among them, OTU0001 was enriched on all three types of biochar compared with the bulk soil and had a high relative abundance ranging from

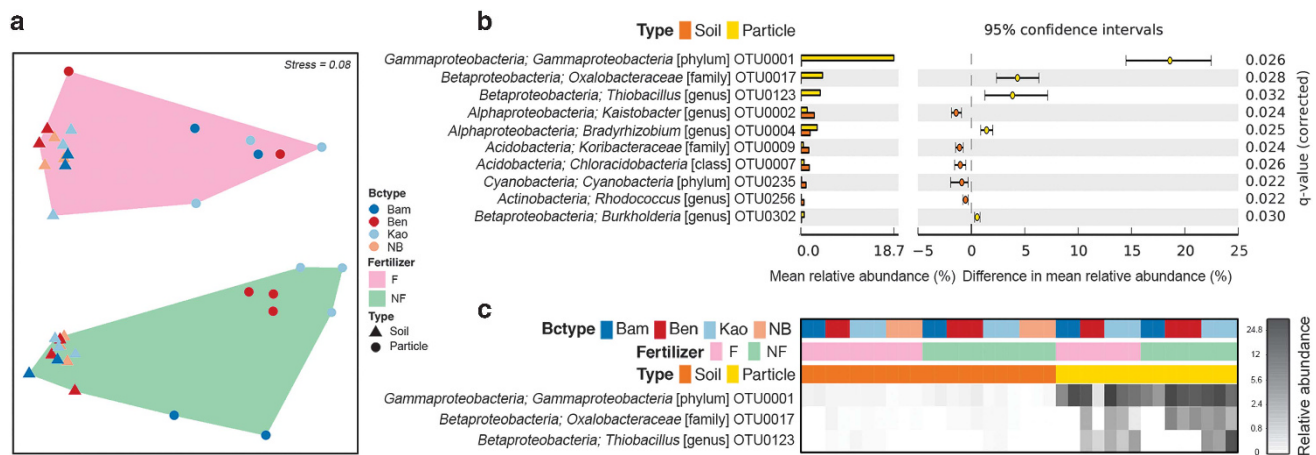


Figure 1 (a) Non-metric multidimensional scaling plot illustrating the similarities between individual samples based on Bray–Curtis distance of bacterial community structures. Relative abundances of bacterial taxa were square-root transformed before calculating the Bray–Curtis distance. (b) Extended error bar plot showing the ten most abundant OTUs that had significant differences between bulk soils and biochar particles. Positive differences in mean relative abundance indicate OTUs overrepresented on the biochar particles, while negative differences indicate greater abundance in bulk soil. (c) The relative abundance of the three most abundant OTUs on biochar particles across all samples. For b and c, the OTU names are formatted as: name of class level; name of the lowest classified level (the lowest classified level). A completed heatmap is provided as Supplementary Figure 2.

7.37 to 27.52% (with the exception of one Ben-F-particle sample being only 0.68%; Figure 1c). Without fertilization, the relative abundance of OTU0001 on Bam ($9.56 \pm 2.20\%$, mean \pm s.e.m.) was also significantly lower than on Kao ($20.94 \pm 2.57\%$) and Ben ($21.74 \pm 1.66\%$). OTU0017 (*Oxalobacteraceae*, class Betaproteobacteria) was enriched only on MEB particles ($7.61 \pm 1.01\%$ without fertilizer and $3.13 \pm 1.23\%$ with fertilizer) and below the detection limit in the neat biochar. The representative 16S rRNA sequence of OTU0017 was 98% similar to a uncharacterized and unpublished bacterium isolated from tungsten sand tailings (Genbank accession no. JQ608321; Supplementary Figure 3) and less than 93% similar to the nearest characterized isolate, *Herbaspirillum massiliense* JC206, which was isolated from stool (Lagier *et al.*, 2012). OTU0123 (*Thiobacillus*, class Betaproteobacteria) was abundant on the Kao particles ($8.47 \pm 3.00\%$) and only detected on the Ben particles in the presence of fertilizer ($2.14 \pm 0.81\%$). The representative 16S rRNA sequence of OTU0123 was 98% similar to *Thiobacillus thioparus* strain THI 111 (Genbank accession no. NR_117864).

Our 16S rRNA survey is consistent with a recent study on the surface microbiota of a corn cob biochar (Sun *et al.*, 2016), which also observed a strong enrichment of specific taxa, especially for Proteobacteria (Figure 1b). We further show here that the presence of clay minerals and iron sulfate on the biochar influences the bacterial community composition on the surface by specifically enriching two Betaproteobacteria (Figures 1b and c). A previous study has seen a similar enrichment of this bacterial class on clay minerals in artificial soils (Ding *et al.*, 2013). Collectively, this shows that deterministic processes govern the assembly of communities on biochar, which offers the potential to design MEBs that specifically enrich certain kind of bacteria.

Gammaproteobacterium OTU0001—a representative of a new, divergent bacterial clade

The prevalence of OTU0001 on all three types of biochar particles and its low-level taxonomic assignment (that is, class Gammaproteobacteria) led us to further investigate its phylogeny in comparison to related isolates and uncultured organisms (Figure 2). OTU0001 falls into a cluster of uncultured bacteria that were all found in carbonaceous environments. Specifically, the 16S rRNA gene sequence of OTU0001 was identical to an uncultured bacterium found to be enriched on the surface of a biocathode in a microbial fuel cell (Sun *et al.*, 2012). This biocathode was made from a semicoke, which was obtained from the carbonization of organic matter below 700 °C, similar to the condition of pyrolysis used here to produce biochar. Other sequences in this cluster were from a cathodic carbon fiber paper (JN802222; Xia *et al.*, 2012), a submicronic filter of hemodialysis (AM087517; Gomila *et al.*, 2006) and activated carbon filters (DQ646451, JQ237904, JQ926658; Hwang *et al.*, 2006; Liao *et al.*, 2012, 2013). Overall this shows that OTU0001 represents a new gammaproteobacterial group of uncultured bacteria, whose members are often associated with carbonized materials that can deliver electrons to cells. This novel group was only distantly related (about 10% 16S rRNA gene sequence divergence) to a cluster of cultured organisms that was defined by *Acidiferrobacter thiooxydans*, which is an acidophilic iron-oxidizing bacterium (Hallberg *et al.*, 2011).

Genomic function of the biochar-enriched Gammaproteobacterium

To gain insight into the functional properties of the three biochar/MEB-enriched OTUs, we reconstructed their genomes from metagenomic data (Table 2). A draft genome classified to the class

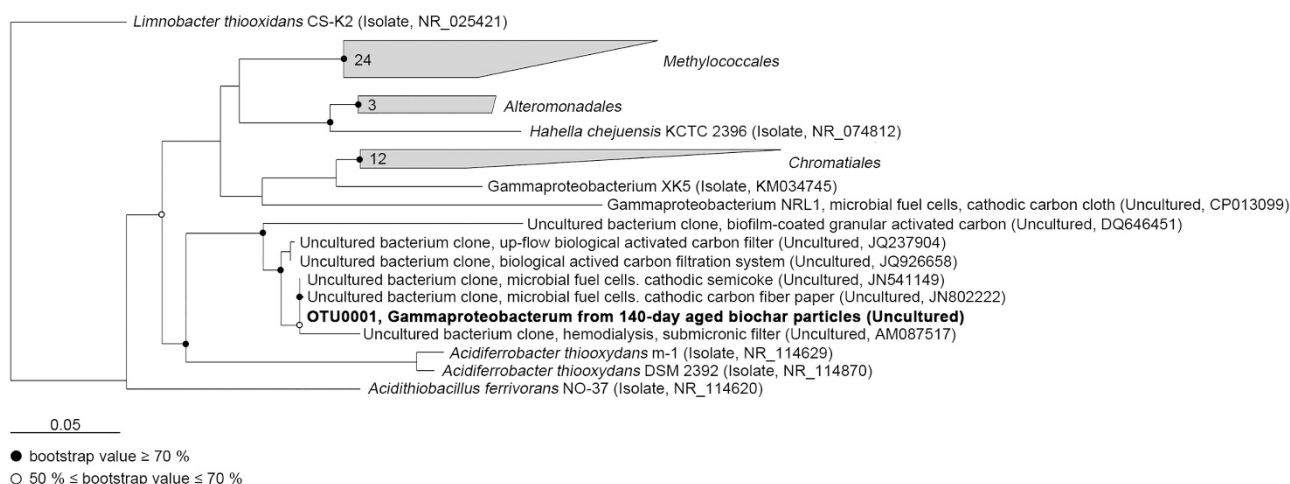


Figure 2 Phylogenetic tree based on the OTU0001's partial 16S rRNA gene sequence (482 nucleotides) and 16S rRNA gene sequences from related organisms. For clarity, only the immediate neighborhood of the OTU0001's clade is shown. The scale bar represents 5% nucleotide substitutions.

Table 2 Summary of Gama1, Oxal1 and Thio1 genome sequences

	<i>Gama1</i>	<i>Oxal1</i>	<i>Thio1</i>
Completeness ^a	88.4	99.2	100
Contamination	2.23	2.27	0.31
Total length (base pairs)	2 733 588	3 773 333	3 303 696
GC content	62.69%	57.33%	62.49%
Number of scaffolds	181	27	33
Coding density	89.30%	86.81%	91.98%
Average coverage	315.96	136.34	133.00
16S rRNA sequence	Yes	No	No
Taxonomic classification ^b	Gammaproteobacteria [C]	Oxalobacteraceae [F]	Thiobacillus [G]

^aBased on lineage-specific marker sets determined with CheckM. ^bTo the lowest classified level given by Phylsift.

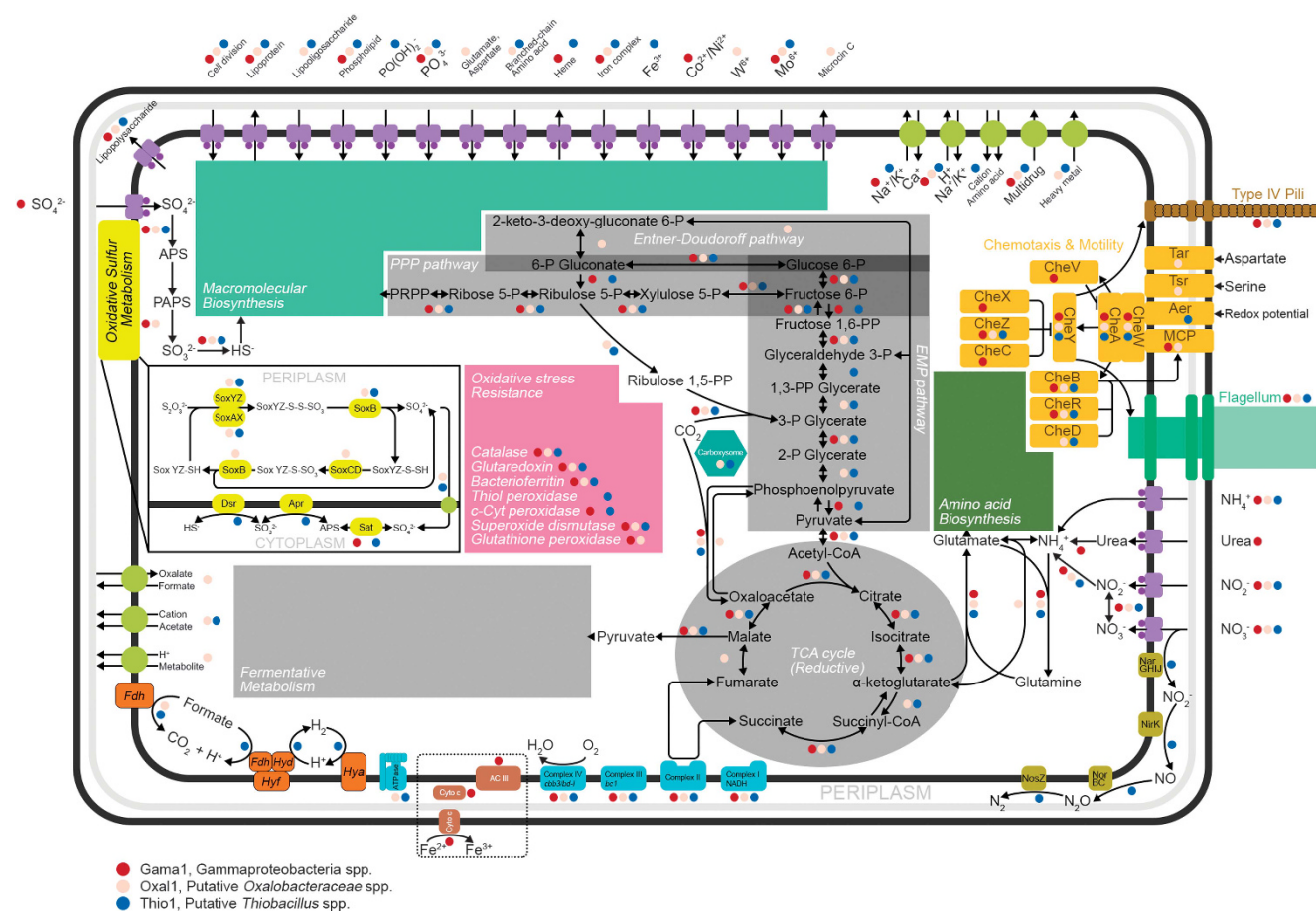


Figure 3 Metabolic reconstructions of the three dominant bacteria (that is, Gama1, Oxal1 and Thio1) on biochar and mineral-enriched biochar particles. Presence of genes and pathways in a given bacterial genome is indicated by colored dots (legend at lower left).

Gammaproteobacteria by Phylsift and with 88.44% completeness was recovered. The genome termed Gama1 had the highest average sequencing coverage (316 ×) among all recovered genomes and contained a scaffold with a 63 base pairs terminal end that was identical to the representative 16S rRNA sequence of OTU0001. We therefore assigned the Gama1 genome to the abundant OTU0001.

Analysis of the Gama1 genome revealed genes encoding for the key enzymes involved in carbon

fixation cycle (Calvin-Benson-Basham reductive pentose phosphate pathway, CBB), including the RuBisCo large and small subunits and the RuBisCo activation proteins CbbO, CbbQ and CbbX. We found two types of *RuBisCo* operon arrangements located in different scaffolds. One gene cluster contained the *RuBisCo* large and small subunits followed by *cbbO* and *cbbQ* (scaffold ID: Ga0079483_1120) and another one contained the *RuBisCo* large and small subunits with *cbbX* located downstream (Ga0079483_1110). These two

types of gene arrangements imply Form IAq and Form IC RuBisCo enzymes, respectively (Badger and Bek, 2008), which were further confirmed by maximum likelihood phylogenetic analysis constructed for the RbcL (Supplementary Figure 4). The Form IAq RbcL was 94.69% similar to the one from *Lamprocystis purpurea* DSM 4197 (class *Gammaproteobacteria*), while the Form IC RbcL was 95.49% similar to *Nitrosococcus halophilus* Nc4 (class *Gammaproteobacteria*). Both forms of RuBisCo enzymes are adapted to medium to high CO₂, but Form IAq is more likely to react with O₂ as an alternative substrate than Form IC (Badger and Bek, 2008). This suggests that Gama1 experiences substantial amounts of CO₂ with variable O₂ level on the biochar surface.

The Gama1 genome showed versatility with respect to the uptake of nitrogen resources (Figure 3). We identified a gene cluster containing a urease operon with urea transport genes located downstream (Ga0079483_1050), ammonium, nitrate and nitrite transport genes (Ga0079483_1030 and 1014) as well as assimilatory nitrate reduction genes (Ga0079483_1095). In contrast, ATP-binding cassette transporters and co-transporters for oligosaccharide and branched-chain amino acid were not recovered in the Gama1 genome (Figure 3), indicating an inability to acquire organic compounds from the environment. Furthermore, we did not find genes encoding key enzymes for fermentation, such as lactate dehydrogenase, pyruvate decarboxylase and formate dehydrogenase. These observations suggest that Gama1 has a strictly autotrophic lifestyle.

We found a gene cluster in the Gama1 genome (Ga0079483_1017) encoding for a MobB-containing (molybdopterin oxidoreductase Fe₄S₄ region) alternative respiratory complex III (AC III), which was first proposed to be involved in iron oxidation in the Zetaproteobacterium *Mariprofundus ferrooxydans* PV-1 (Singer *et al.*, 2011a, 2013). Gene for the AC III have also recently been found in the Gammaproteobacterium NRL1 (Wang *et al.*, 2015), which shared 88% 16S rRNA gene identity with OTU0001 (Figure 2). The conceptual iron oxidation pathway by Singer *et al.* (2013) proposed an outer membrane c-type cytochrome (c-Cyt) and a periplasmic c-Cyt to be involved in electron transfer. We also observed a gene cluster that consecutively encoded for a c-Cyt biogenesis system, two c-Cyt family proteins with doubled CXXCH heme-binding motifs, three periplasmic triheme c-Cyt, two porin-like outer membrane proteins and a 2Fe-2S ferredoxin (Ga0079483_1028; Supplementary Figure 5). This operon structure indicates its potential to encode a porin-cytochrome protein complex for trans-outer-membrane electron transport, similar to what has been described in *Shewanella* and *Geobacter* (Lovley *et al.*, 2004; Clarke *et al.*, 2011; Richardson *et al.*, 2012; Liu *et al.*, 2014). A similar genomic arrangement around the periplasmic triheme c-Cyt gene in this operon (Ga0079483_1028) was also found in an iron-oxidizing bacterium *Leptothrix cholodnii* SP-6

(Genbank accession no. NC_010524; Supplementary Figure 5). The porin-cytochrome protein complex might thus function as the outer membrane c-Cyt and periplasmic c-Cyt in the iron oxidation pathway to conduct electrons from extracellular reduced iron into the electron transport chain (Wang *et al.*, 2015).

The Gama1 genome also encodes for cbb₃-type cytochrome c oxidases and a cytochrome bd-I ubiquinol oxidase, which have high affinities for O₂ and can thus support growth under microaerophilic conditions (Jünemann, 1997; Buschmann *et al.*, 2010). Reactive oxygen species, such as superoxide anion radicals, hydrogen peroxide and hydroxyl radicals, are generated during aerobic iron oxidation (Cabisco *et al.*, 2010). A series of genes encoding for antioxidants were identified in the Gama1 genome (Supplementary Table S2), including five copies of the cytochrome c peroxidase and two copies of bacterioferritins. Cytochrome c peroxidases can reduce hydrogen peroxide to water, and have been suggested to be vital during the iron oxidation in *Marinobacter aquaeolei* (Singer *et al.*, 2011b; Waite, 2012). Bacterioferritin is an iron-storage protein and is critical for detoxification of harmful iron and oxygen species associated with iron oxidation (Carrondo, 2003).

Although we did not observe homologs to some well-known genes involved in iron oxidation, such as *rus*, *pioABC*, *foxEYZ* in Gama1 (Bird *et al.*, 2011), based on the putative iron oxidation pathways found, as well as greater enrichment of Gama1 on the ferrous sulfate treated biochar particles (Kao and Ben) in comparison to untreated biochar particles (Bam, Table 1; Figure 1c), we propose that the dominant Gama1 oxidizes iron by combining an AC III and porin-cytochrome protein complex (Figure 3). Electrons from iron oxidation could then be transferred to O₂, which generates NADH and ATP to support autotrophic growth.

Interaction of Gama1 with iron on the biochar

The genome-based evidence for iron oxidation by Gama1 would predict that the bacterium is located near iron on the biochar structure. We therefore investigated the physical localization of the Gama1 on the biochar surface using GISH (Ye *et al.*, 2015) and investigated the elemental distributions and redox states around the bacterium by EDS and EELS.

The probe targeting the 16S rRNA gene sequence of OTU0001 hybridized to rod-shaped cells (Figure 4a) through dense deposition of nanogold particles (Figure 4b). While gold signals were also observed outside of cell structures, they were dispersed and lumpy, which was likely caused by non-specific binding of nanogold to charged minerals as has been previously reported (Ehrhardt *et al.*, 2009). We also observed pili-like structures on these rod-shaped cells (Figure 4a; arrows), consistent with the Gama1 genome encoding for pili (Figure 3; Supplementary Information). An EDS spectrum revealed the iron peak in the region around the Gama1 cells (Figure 4c). Other cell

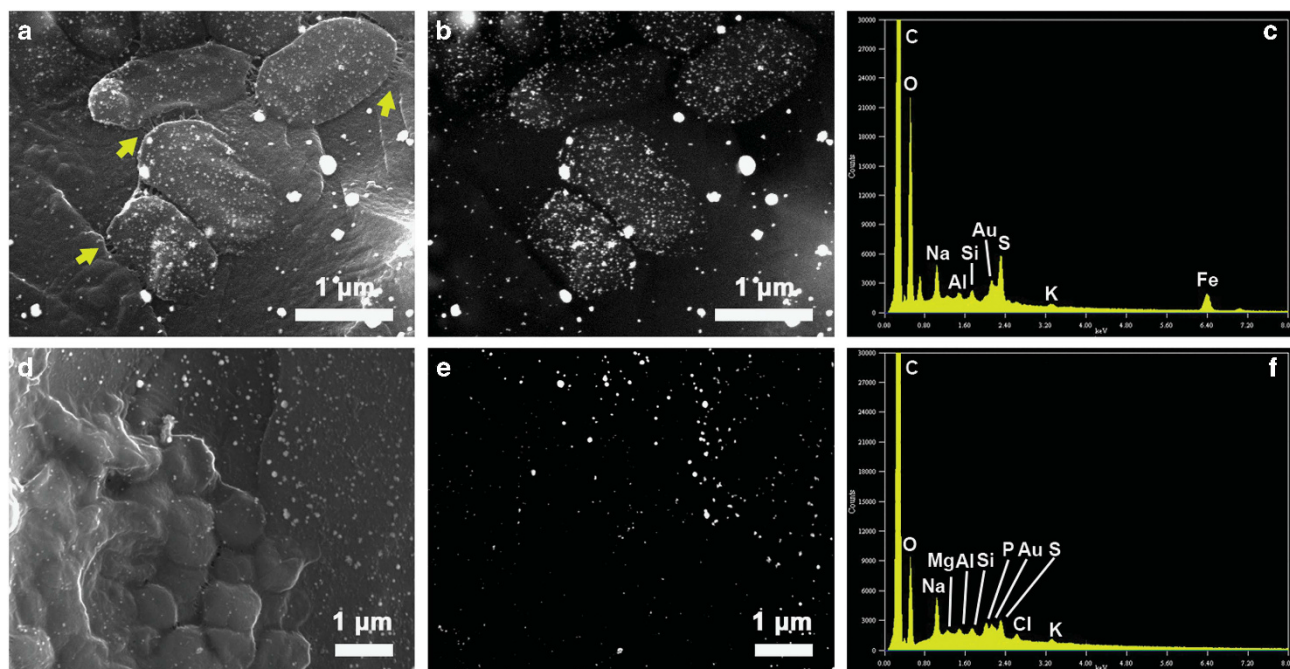


Figure 4 Electron micrographs of GISH for OTU0001 on a mineral-enriched biochar particle. (a) and (d) represent GISH-labeled and -unlabeled cells, respectively, under secondary electron mode. The yellow arrows in a point to extracellular pili-like structures. (b) and (e) represent GISH-labeled and -unlabeled cells, respectively, under backscattered electron mode, which shows a denser and more regular accumulation of nanogold particles inside the cell compared to the surroundings. (c) and (f) correspond to the elemental spectrum using the EDS for (a) and (d), respectively.

morphotypes without nanogold signal were also found on the same biochar particles (Figures 4d and e), but lacked an iron signal in their vicinity (Figure 4f). This result shows a specific localization of Gama1 in iron-rich regions of the biochar.

To further support the notion of iron oxidation by Gama1, we investigated the iron species that are directly in contact with the cells using HAADF imaging in STEM combined with EDS to allow SI mapping with a nanometer scale resolution. An EELS was simultaneously conducted to investigate the oxidation state of the iron (Chen *et al.*, 2009). The bright-field and HAADF images show a nanogold-labeled Gama1 cell next to a particle (Figures 5a and b). We then conducted SI mapping to determine the element distributions of the cell and the particle (Figure 5a, yellow rectangle). The EDS spectrum shows a strong Au signal (Figure 5c) consistent with the cell being labeled with nanogold as well as signals for C, N and O (Figure 5d), as would be expected for cellular matter. The particle has three main phases (Figures 5e–g), which all have similar qualitative elemental composition of C, O, Mg, Si, S and Fe. This observation indicates that the particle consists of a complex organo-mineral phase. However, the local Fe/O ratios of these three phases are distinct from each other, with the largest ratio being away from the cell (Figure 5e) and the smallest ratio seen for the region directly in contact with the cell (Figure 5g). This indicates a more reduced state of Fe species at

the distal part of the particle, and a more oxidized state of Fe species in the region directly in contact with the Gama1 cell (Figure 5h). The EELS analysis of the Fe $2p$ $L_{2,3}$ edge from the proximal area to the Gama1 cell (Figure 5b, inset) showed a small pre-peak in the L_3 edge (see yellow arrow in inset) and a post-peak in the L_2 edge in the region of 710–730 eV, indicating the presence of magnetite (Fe_3O_4), which contains mixed valence of Fe(II) and Fe(III), and a change in the Fe oxidation state towards $\gamma\text{-Fe}_2\text{O}_3$ or $\alpha\text{-Fe}_2\text{O}_3$ (Almeida *et al.*, 2014). These observations together further support the notion of active iron oxidation by Gama1, which is taking place on the interface with an iron-containing organo-mineral particle.

The genes putatively involved in the iron oxidation pathway of Gama1 have also been recently proposed to be involved in the extracellular electron uptake from a cathode in the Gammaproteobacterium NRL1 (Wang *et al.*, 2015). We performed cyclic voltammetry on Bam and the two MEBs (Supplementary Information; Supplementary Figure 6) and found that the MEBs are considerably more redox active than the Bam. Kao, Ben and Bam are however all able to store and conduct significant amounts of charge. Previous research has found that redox active magnetic nanoparticles (for example, Fe_3O_4) can be important for interspecies electron transfer (Aulenta *et al.*, 2013; Klüpfel *et al.*, 2014a, b). Measurements of magnetic hysteresis loops show that Kao and Ben have a significant concentration of

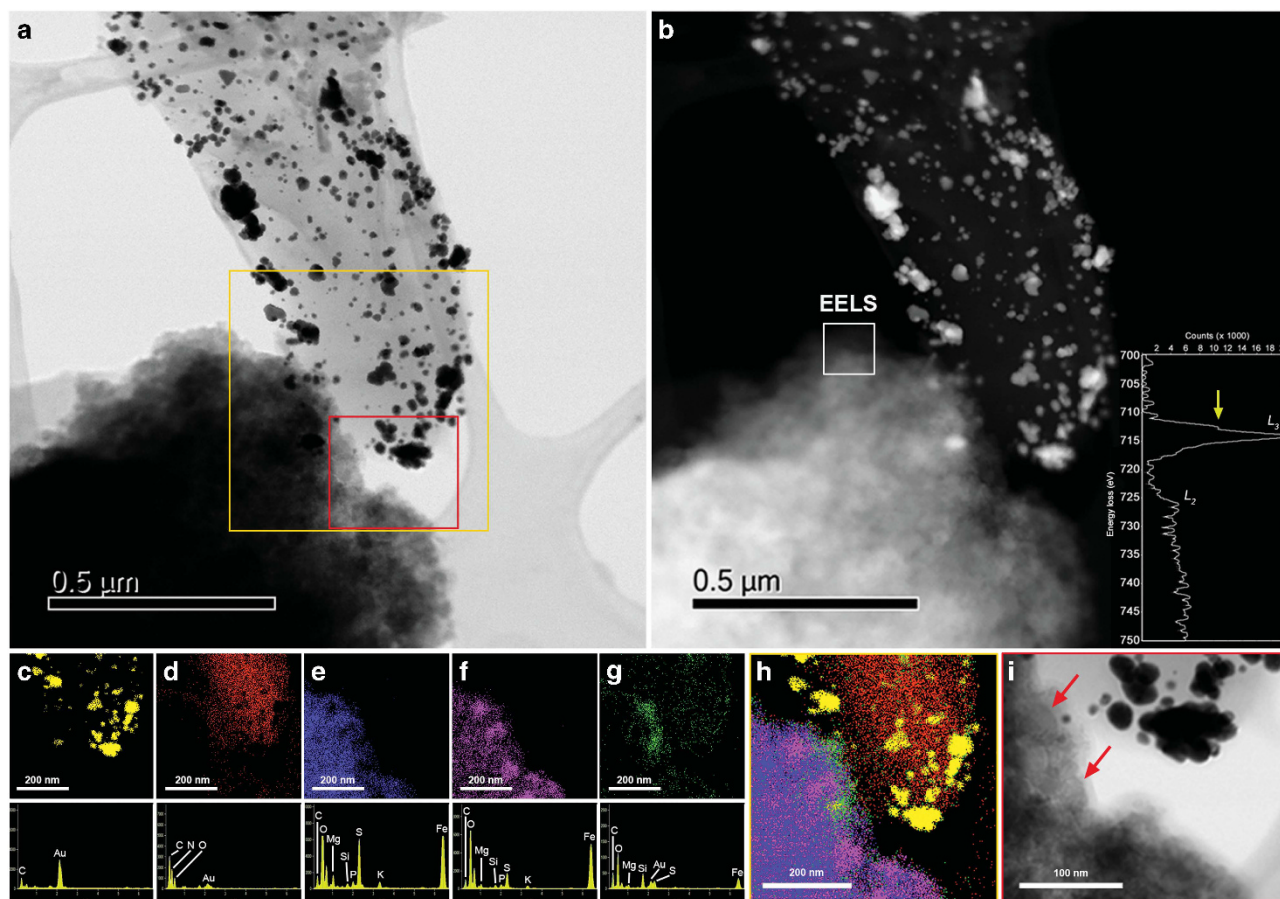


Figure 5 Image of (a) a bright-field STEM and (b) a HAADF analysis acquired for a GISH-labeled Gama1 cell in contact with an organo-mineral particle. Associated EELS spectrum acquired from the edge of the mineral grain are shown in the inset of b. (c–g) show EDS SI mapping for the area selected in the yellow rectangle seen in a. The spectrum below each image represents the corresponding EDS analysis. The peak at the right side of the O signal is the secondary peak of Fe. (h) shows a superimposed image of c–g. (i) An enlarged area from the red rectangle in a showing magnetite iron particles (arrows). The netlike structure in a is the carbon grid for holding the specimen

superparamagnetic nanoparticles, whereas Bam does not (Supplementary Information; Supplementary Figures 7 and 8). Nanoscale examination of the surface of the biochar shows that magnetite particles below 20 nm in size are in direct contact with the Gama1 bacterium (Figure 5i, red arrows). These magnetic iron nanoparticles could reduce the activation energy for redox reactions to take place and increase the rate of charge transfer (Peng *et al.*, 2013; Yin *et al.*, 2013). We therefore propose that Gama1 may gain adequate electrons not only through the direct contact with superparamagnetic iron nanoparticles, but also from electrons that are produced in redox reactions in proximal parts and then conducted through the biochar structure (Joseph *et al.*, 2015). The higher amount of superparamagnetic iron nanoparticles on Kao and Ben and its associated reduction in activation energy for electron transfer could also explain why the iron-oxidizing Gama1 bacterium is more enriched on these two MEBs (~20% relative abundance; see above) when compared with Bam (~10%).

A predicted mixotrophic lifestyle of the MEB-enriched Oxalobacteraceae and Thiobacillus

Our metagenomic dataset also contained nearly complete genome sequences assigned to the family *Oxalobacteraceae* and the genus *Thiobacillus*, respectively (Table 2). These were termed Oxal1 and Thio1 and assigned to OTU0017 and OTU0123, respectively. Similar to Gama1, Oxal1 and Thio1 also have complete gene sets for the CBB pathway to carry out carbon fixation (Figure 3). The genomes of Oxal1 and Thio1 harbor genes encoding large and small subunits of RuBisCo (Oxal1: Ga0079480_116, Thio1: Ga0079481_105). The *RuBisCo* genes of Oxal1 were classified as Form IAc, whereas Thio1 has two sets of genes for Form IAq and Form II RuBisCo (Supplementary Figure 4). In general, Form IAc RuBisCo is adapted to low CO₂ environment, while Form IAq and II RuBisCo are adapted to medium to high CO₂ environment (Badger and Bek, 2008). In addition, operons encoding carboxysome shell proteins and shell carbonic anhydrase were detected in Oxal1 and Thio1 (Supplementary

Figure 4). Carboxysomes are well-known for their role in encapsulating RuBisCo and carbonic anhydrase, and thereby enhancing carbon fixation by elevating the levels of CO₂ in the vicinity of RuBisCo (Yeates *et al.*, 2008).

Reconstruction of central metabolic pathways of Oxal1 and Thio1 revealed essential genes for the glycolysis and tricarboxylic acid cycle (Figure 3). In addition, Oxal1 possesses genes for the Entner–Doudoroff pathway. Several ATP-binding cassette transporters for branched-chain amino acid, C4-dicarboxylate and oligosaccharide, as well as amino acid and oxalate co-transporters were found in Oxal1 and Thio1 (Figure 3). We also identified genes encoding for enzymes involved in the degradation of complex organic substrates, including aromatic dioxygenases (Oxal1, Ga0079480_102), protocatechuate-3,4-dioxygenase (Oxal1, Ga0079480_110), toluene monooxygenase (Thio1, Ga0079481_113) and methanesulfonate monooxygenase (Thio1, Ga0079481_113). Acidic, aromatic and phenolic carbon compounds have previously been found by Nuclear Magnetic Resonance analysis in the two MEBs used here (Rawal *et al.*, 2016) and we found that Ben and Kao contains higher amounts of dissolved organic carbon than Bam (Table 1). These organic compounds could be utilized by the enzymes above for by Oxal1 and Thio1 for heterotrophic growth on the Ben and Kao surfaces (Figure 1c).

Energy generation in the MEB-enriched *Oxalobacteraceae* and *Thiobacillus*

Oxal1 and Thio1 were almost exclusively found on the biochar particles treated with ferrous sulfate (Ben and Kao; Figure 1c), which contained about 10× more sulfur than Bam (Table 1). X-ray photoelectron spectrometry showed that a substantial proportion of the sulfur is in reduced form in both fresh and aged Ben and Kao (Supplementary Figure 9). This led us to investigate the sulfur metabolism in these two genomes in more detail. Oxal1 and Thio1 contained gene clusters encoding for enzymes involved in oxidizing thiosulfate to sulfate (Friedrich *et al.*, 2005). Specifically, the *sox* operon in Oxal1 consists of *soxCDYZXAB* (Ga0079480_117) encoding four periplasmic proteins, SoxXA, SoxYZ, SoxB and Sox(CD)₂ (Figure 3), while the *sox* operon in Thio1 only contained *soxXYZAB* (Ga0079481_108). Thio1 also has another two gene clusters comprised of *soxXA* (Ga0079481_133) and *soxC* (Ga0079481_106). Friedrich *et al.* (2000) reported that the Sox system reconstituted from SoxXA, SoxYZ, SoxB and Sox(CD)₂ produced 8 mol of electrons per mol of thiosulfate, while only 2 mol of electrons were produced with the deletion of Sox(CD)₂. The potential absence of *soxCD* in its genome implies that Thio1 likely utilizes other oxidization pathways to obtain electrons. We found a *dsrAB* gene cluster in Thio1 that was similar to the one in *Thiobacillus*

denitrificans ATCC25259 (IMG Genome ID: 637000324, 94% and 98% similarity for *dsrA* and *dsrB*, respectively). The *dsrAB* genes, which encode the siroheme-containing sulfite reductase, has been shown to be involved in the reverse direction for the dissimilatory oxidation of sulfur in *Thiobacillus denitrificans* (Trüper, 1994). This indicates that Thio1 may also use dissimilatory oxidation of sulfur compounds to acquire electrons.

The genomes of Oxal1 and Thio1 also encode all necessary enzymes for aerobic respiration (Figure 3). We identified genes encoding four types of terminal oxidases, including aa₃-, bo₃- and cbb₃-type cytochrome c oxidase, as well as cytochrome bd-I ubiquinol oxidase. Oxal1 contains genes encoding all four types of terminal oxidases, whereas Thio1 harbors genes for three types of terminal oxidases (that is, no bo₃-type cytochrome c oxidase; Supplementary Table 3). It has been shown that both aa₃- and bo₃-type cytochrome c oxidases are only produced under O₂-rich conditions (Haltia *et al.*, 1988; Cotter *et al.*, 1990), while cbb₃-type cytochrome c oxidase and cytochrome bd-I ubiquinol oxidase have high affinities for low levels of O₂ (Jünemann, 1997; Buschmann *et al.*, 2010). Hence, the presence of genes encoding both types of terminal oxidases, functioning under either aerobic or microaerobic conditions, suggests a potential adaptation of Oxal1 and Thio1 to variable O₂ levels. Additionally, Thio1 contained a suite of genes for denitrification, including those encoding for nitrate reductase (*narKKGHJL*, Ga0079481_113), nitrite reductase (*nirK*, Ga0079481_107), nitric oxide reductase (*norZ*, Ga0079481_111) and nitrous oxide reductase (*nosZR*, Ga0079481_113). The capability of using nitrate/nitrite as terminal electron acceptors may also explain the presence of Thio1 on Kao, which has a higher level of total soluble nitrogen and total N compared to the other two biochars (Table 1), as well as on Kao and Ben when monoammonium phosphate was added (Figure 1c). Additional metabolic properties predicted from the genomes of Oxal1 and Thio1 are presented in the Supplementary Information.

Conclusion

In contrast to previous 16S rRNA gene-based functional prediction that xenobiotic degradation was enriched on biochar (Sun *et al.*, 2016), we found that chemolithotrophic and autotrophic metabolisms were characteristic of the abundant bacterial members on the surfaces of biochar and MEBs. A novel, iron-oxidizing Gama1 was found to dominate all surface communities analyzed here. Iron was provided as part of the production for the MEBs and was also likely adsorbed as nanoparticles from the soil onto the biochar surface as previously observed (Lin *et al.*, 2012). Furthermore, the electroconductive properties of biochar (Joseph *et al.*,

2015; Supplementary Information) and the potential ability of direct electron uptake from solid surfaces by the novel Gammaproteobacterium highlight the possibility that chemolithotrophy could also be driven by redox reactions that occur in any part of the biochar or the soil environment. This could include anaerobic processes, where bacteria use the biochar surface as electron acceptors, as has been recently shown in laboratory experiments with *Geobacter sulfurreducens* (Yu *et al.*, 2015). Temporal fluctuation of redox conditions, for example caused by changes in the soil's water saturation, might also allow for biochar or MEB surfaces to be 'recharged' through reductive, metabolic processes, similar to what has been recently observed for the redox cycling of humic acids in soil (Klüpfel *et al.*, 2014a, b).

Such anaerobic, biotic processes were however not dominant in our experimental set-up, which was characterized by oxygen-replete conditions. Instead, the genetic capacity for aerobic respiration was mostly seen in the surface-enriched bacteria. This could allow for aerobic sulfur oxidation to occur in a novel member of the family *Oxalobacteraceae* (Oxal1) and a *Thiobacillus* species (Thio1). The genomes of these two bacteria encode for heterotrophic pathways, which could utilize the complex organic compounds present in MEBs. Their heterotrophic metabolism would also lead to the enrichment of these two bacteria on the MEBs in comparison to the apparently strict autotrophic Gammaproteobacterium (Figure 1c). However, both the *Oxalobacteraceae* and *Thiobacillus* bacteria, in the same way as the Gammaproteobacterium, may have an extended genetic capacity to CO₂ fixation. This indicates that bacteria on the surface of biochar are indeed limited by available organic substrates. Biochars have both labile and recalcitrant organic compounds (Bruun *et al.*, 2011) and the microbial observations made here indicate that the metabolizable organic fractions might be largely depleted within the 140 days incubation in our experimental set-up. Long-term exposure of biochar to the soil will also likely deplete organic compounds suitable to support heterotrophic growth. Biochar and MEB can then support chemolithotrophic processes that provide reductive energy to fuel carbon fixation. Our results thus provide a microbial mechanism why biochars often have negligible effect on soil respiration (Liu *et al.*, 2016), but instead supports carbon sequestration (Lehmann *et al.*, 2006; Woolf *et al.*, 2010). Designing biochars and mineral-enriched biochars in the future to improve these kind of microbially mediated redox reactions and carbon sequestration has a great potential for managing the soil environment.

Conflict of Interest

The authors declare no conflict of interest.

Acknowledgements

We acknowledge Dr Simon Hager from the Electron Microscopy Unit and Dr Bill Bin Gong from the Solid State and Elemental Analysis Unit at UNSW for technical support. We thank Professor Gene Tyson (Australian Centre for Ecogenomics) for advice on the metagenomic sequencing. We also thank Professor Xiaohua Zhang (Ocean University of China) for kindly providing strain *Catenovulum agarivorans* YM01. JY would like to thank the support of China Scholarship Council (File ID: 201206230085). This research was supported by the Australian Research Council (LP120200418) and Renewed Carbon Pty Ltd.

References

- Abujabbar IS, Bound SA, Doyle R, Bowman JP. (2016). Effects of biochar and compost amendments on soil physico-chemical properties and the total community within a temperate agricultural soil. *Appl Soil Ecol* **98**: 243–253.
- Almeida TP, Kasama T, Muxworthy AR, Williams W, Nagy L, Hansen TW *et al.* (2014). Visualized effect of oxidation on magnetic recording fidelity in pseudo-single-domain magnetite particles. *Nat Commun* **5**: 5154.
- Anderson CR, Condon LM, Clough TJ, Fiers M, Stewart A, Hill RA *et al.* (2011). Biochar induced soil microbial community change: implications for biogeochemical cycling of carbon, nitrogen and phosphorus. *Pedobiologia* **54**: 309–320.
- Anderson MJ, Gorley RN, Clarke KR. (2008). *PERMANOVA + for PRIMER: Guide to Software and Statistical Methods* 1st edn, PRIMER-E Ltd: Plymouth, UK.
- Aulenta F, Rossetti S, Amalfitano S, Majone M, Tandoi V. (2013). Conductive magnetite nanoparticles accelerate the microbial reductive dechlorination of trichloroethene by promoting interspecies electron transfer processes. *ChemSusChem* **6**: 433–436.
- Badger MR, Bek EJ. (2008). Multiple Rubisco forms in proteobacteria: their functional significance in relation to CO₂ acquisition by the CBB cycle. *J Exp Bot* **59**: 1525–1541.
- Bardgett RD, van der Putten WH. (2014). Belowground biodiversity and ecosystem functioning. *Nature* **515**: 505–511.
- Bird LJ, Bonnefoy V, Newman DK. (2011). Bioenergetic challenges of microbial iron metabolisms. *Trends Microbiol* **19**: 330–340.
- Bruun EW, Hauggaard-Nielsen H, Ibrahim N, Egsgaard H, Ambus P, Jensen PA *et al.* (2011). Influence of fast pyrolysis temperature on biochar labile fraction and short-term carbon loss in a loamy soil. *Biomass Bioenergy* **35**: 1182–1189.
- Buschmann S, Warkentin E, Xie H, Langer JD, Ermler U, Michel H. (2010). The structure of cbb3 cytochrome oxidase provides insights into proton pumping. *Science* **329**: 327–330.
- Cabiscol E, Tamarit J, Ros J. (2010). Oxidative stress in bacteria and protein damage by reactive oxygen species. *Int Microbiol* **3**: 3–8.
- Cao X, Ma L, Liang Y, Gao B, Harris W. (2011). Simultaneous immobilization of lead and atrazine in

- contaminated soils using dairy-manure biochar. *Environ Sci Technol* **45**: 4884–4889.
- Carrondo MA. (2003). Ferritins, iron uptake and storage from the bacterioferritin viewpoint. *EMBO J* **22**: 1959–1968.
- Chen S-Y, Gloter A, Zobelli A, Wang L, Chen C-H, Colliex C. (2009). Electron energy loss spectroscopy and ab initio investigation of iron oxide nanomaterials grown by a hydrothermal process. *Phys Rev B* **79**: 104103.
- Chia C, Munroe P, Joseph S, Lin Y, Lehmann J, Muller D et al. (2012). Analytical electron microscopy of black carbon and microaggregated mineral matter in Amazonian dark Earth. *J Microsc* **245**: 129–139.
- Chia CH, Singh BP, Joseph S, Graber ER, Munroe P. (2014). Characterization of an enriched biochar. *J Anal Appl Pyrol* **108**: 26–34.
- Chia CH, Downie A, Munroe P. (2015). Characteristics of biochar: physical and structural properties. In: Lehmann J, Joseph S (eds). *Biochar for Environmental Management: Science and Technology* 2nd edn, Earthscan Books Ltd: London, pp 89–109.
- Clarke TA, Edwards MJ, Gates AJ, Hall A, White GF, Bradley J et al. (2011). Structure of a bacterial cell surface decaheme electron conduit. *Proc Natl Acad Sci USA* **108**: 9384–9389.
- Cotter PA, Chepuri V, Gennis R, Gunsalus R. (1990). Cytochrome o (cyoABCDE) and d (cydAB) oxidase gene expression in *Escherichia coli* is regulated by oxygen, pH, and the fnr gene product. *J Bacteriol* **172**: 6333–6338.
- Darling AE, Jospin G, Lowe E, Matsen FA IV, Bik HM, Eisen JA. (2014). PhyloSift: phylogenetic analysis of genomes and metagenomes. *PeerJ* **2**: e243.
- Ding G-C, Pronk GJ, Babin D, Heuer H, Heister K, Kögel-Knabner I et al. (2013). Mineral composition and charcoal determine the bacterial community structure in artificial soils. *FEMS Microbiol Ecol* **86**: 15–25.
- Ehrhardt C, Haymon R, Sievert SM, Holden P. (2009). An improved method for nanogold in situ hybridization visualized with environmental scanning electron microscopy. *J Microsc* **236**: 5–10.
- Feng Y, Xu Y, Yu Y, Xie Z, Lin X. (2012). Mechanisms of biochar decreasing methane emission from Chinese paddy soils. *Soil Biol Biochem* **46**: 80–88.
- Fierer N, Jackson RB. (2006). The diversity and biogeography of soil bacterial communities. *Proc Natl Acad Sci USA* **103**: 626–631.
- Friedrich CG, Quentmeier A, Bardischewsky F, Rother D, Kraft R, Kostka S et al. (2000). Novel genes coding for lithotrophic sulfur oxidation of *Paracoccus pantotrophus* GB17. *J Bacteriol* **182**: 4677–4687.
- Friedrich CG, Bardischewsky F, Rother D, Quentmeier A, Fischer J. (2005). Prokaryotic sulfur oxidation. *Curr Opin Microbiol* **8**: 253–259.
- Gomila M, Gasco J, Gil J, Bernabeu R, Inigo V, Lalucat J. (2006). A molecular microbial ecology approach to studying hemodialysis water and fluid. *Kidney Int* **70**: 1567–1576.
- Hallberg KB, Hedrich S, Johnson DB. (2011). *Acidiferrobacter thiooxydans*, gen. nov. sp. nov.; an acidophilic, thermo-tolerant, facultatively anaerobic iron-and sulfur-oxidizer of the family *Ectothiorhodospiraceae*. *Extremophiles* **15**: 271–279.
- Haltia T, Puustinen A, Finel M. (1988). The *Paracoccus denitrificans* cytochrome aa3 has a third subunit. *Eur J Biochem* **172**: 543–546.
- Harter J, Krause H-M, Schuettler S, Ruser R, Fromme M, Scholten T et al. (2014). Linking N₂O emissions from biochar-amended soil to the structure and function of the N-cycling microbial community. *ISME J* **8**: 660–674.
- Hemkemeyer M, Christensen BT, Martens R, Tebbe CC. (2015). Soil particle size fractions harbour distinct microbial communities and differ in potential for microbial mineralisation of organic pollutants. *Soil Biol Biochem* **90**: 255–265.
- Hwang C, Wu W-M, Gentry T, Carley J, Carroll S, Schadt C et al. (2006). Changes in bacterial community structure correlate with initial operating conditions of a field-scale denitrifying fluidized bed reactor. *Appl Microbiol Biotechnol* **71**: 748–760.
- Jeffery S, Verheijen F, Van Der Velde M, Bastos A. (2011). A quantitative review of the effects of biochar application to soils on crop productivity using meta-analysis. *Agric Ecosyst Environ* **144**: 175–187.
- Joseph S, Husson O, Graber ER, Van Zwielen L, Taherymoosavi S, Thomas T et al. (2015). The electrochemical properties of biochars and how they affect soil redox properties and processes. *Agronomy* **5**: 322–340.
- Jünemann S. (1997). Cytochrome bd terminal oxidase. *Biochim Biophys Acta* **1321**: 107–127.
- Kang DD, Froula J, Egan R, Wang Z. (2015). MetaBAT, an efficient tool for accurately reconstructing single genomes from complex microbial communities. *PeerJ* **3**: e1165.
- Klöpffel L, Keiluweit M, Kleber M, Sander M. (2014a). Redox properties of plant biomass-derived black carbon (biochar). *Environ Sci Technol* **48**: 5601–5611.
- Klöpffel L, Piepenbrock A, Kappler A, Sander M. (2014b). Humic substances as fully regenerable electron acceptors in recurrently anoxic environments. *Nat Geosci* **7**: 195–200.
- Kolton M, Harel YM, Pasternak Z, Graber ER, Elad Y, Cytryn E. (2011). Impact of biochar application to soil on the root-associated bacterial community structure of fully developed greenhouse pepper plants. *Appl Environ Microbiol* **77**: 4924–4930.
- Kozich JJ, Westcott SL, Baxter NT, Highlander SK, Schloss PD. (2013). Development of a dual-index sequencing strategy and curation pipeline for analyzing amplicon sequence data on the MiSeq Illumina sequencing platform. *Appl Environ Microbiol* **79**: 5112–5120.
- Krzywinski M, Altman N. (2014). Points of significance: comparing samples-part II. *Nat Methods* **11**: 355–356.
- Kumar S, Nei M, Dudley J, Tamura K. (2008). MEGA: a biologist-centric software for evolutionary analysis of DNA and protein sequences. *Brief Bioinform* **9**: 299–306.
- Lagier J-C, Gimenez G, Robert C, Raoult D, Fournier P-E. (2012). Non-contiguous finished genome sequence and description of *Herbaspirillum massiliense* sp. nov. *Stand Genomic Sci* **7**: 200–209.
- Langille MG, Zaneveld J, Caporaso JG, McDonald D, Knights D, Reyes JA et al. (2013). Predictive functional profiling of microbial communities using 16S rRNA marker gene sequences. *Nat Biotechnol* **31**: 814–821.
- Langmead B, Salzberg SL. (2012). Fast gapped-read alignment with Bowtie 2. *Nat Methods* **9**: 357–359.
- Larkin MA, Blackshields G, Brown N, Chenna R, McGettigan PA, McWilliam H et al. (2007). Clustal W and Clustal X version 2.0. *Bioinformatics* **23**: 2947–2948.
- Lehmann J, Gaunt J, Rondon M. (2006). Bio-char sequestration in terrestrial ecosystems—a review. *Mitig Adapt Strategies Glob Chang* **11**: 395–419.

- Lehmann J, Rillig MC, Thies J, Masiello CA, Hockaday WC, Crowley D. (2011). Biochar effects on soil biota—a review. *Soil Biol Biochem* **43**: 1812–1836.
- Lehmann J, Joseph S. (2015). *Biochar for Environmental Management: Science, Technology and Implementation* 2nd edn. Routledge: London and New York.
- Liao X, Chen C, Chang C-H, Wang Z, Zhang X, Xie S. (2012). Heterogeneity of microbial community structures inside the up-flow biological activated carbon (BAC) filters for the treatment of drinking water. *Biotechnol Bioprocess Eng* **17**: 881–886.
- Liao X, Chen C, Wang Z, Wan R, Chang C-H, Zhang X et al. (2013). Changes of biomass and bacterial communities in biological activated carbon filters for drinking water treatment. *Process Biochem* **48**: 312–316.
- Lin Y, Munroe P, Joseph S, Kimber S, Van Zwieten L. (2012). Nanoscale organo-mineral reactions of biochars in ferrosol: an investigation using microscopy. *Plant Soil* **357**: 369–380.
- Liu X, Zheng J, Zhang D, Cheng K, Zhou H, Zhang A et al. (2016). Biochar has no effect on soil respiration across Chinese agricultural soils. *Sci Total Environ* **554**: 259–265.
- Liu Y, Wang Z, Liu J, Levar C, Edwards MJ, Babauta JT et al. (2014). A trans-outer membrane porin-cytochrome protein complex for extracellular electron transfer by *Geobacter sulfurreducens* PCA. *Environ Microbiol Rep* **6**: 776–785.
- Lovley DR, Holmes DE, Nevin KP. (2004). Dissimilatory fe (iii) and mn (iv) reduction. *Adv Microb Physiol* **49**: 219–286.
- Markowitz VM, Chen I-MA, Palaniappan K, Chu K, Szeto E, Grechkin Y et al. (2012). IMG: the integrated microbial genomes database and comparative analysis system. *Nucleic Acids Res* **40**: D115–D122.
- Mills AL. (2003). Keeping in touch: microbial life on soil particle surfaces. *Adv Agron* **78**: 1–43.
- Morgulis A, Coulouris G, Raytselis Y, Madden TL, Agarwala R, Schäffer AA. (2008). Database indexing for production MegaBLAST searches. *Bioinformatics* **24**: 1757–1764.
- Nielsen S, Minchin T, Kimber S, van Zwieten L, Gilbert J, Munroe P et al. (2014). Comparative analysis of the microbial communities in agricultural soil amended with enhanced biochars or traditional fertilisers. *Agric Ecosyst Environ* **191**: 73–82.
- O'Neill B, Grossman J, Tsai M, Gomes J, Lehmann J, Peterson J et al. (2009). Bacterial community composition in Brazilian anthrosols and adjacent soils characterized using culturing and molecular identification. *Microb Ecol* **58**: 23–35.
- Oksanen J, Blanchet FG, Kindt R, Legendre P, Minchin PR, O'Hara RB et al. (2015). vegan: Community Ecology package. *R package version 2*: 2–1.
- Parks DH, Tyson GW, Hugenholtz P, Beiko RG. (2014). STAMP: statistical analysis of taxonomic and functional profiles. *Bioinformatics* **30**: 3123–3124.
- Parks DH, Imelfort M, Skennerton CT, Hugenholtz P, Tyson GW. (2015). CheckM: assessing the quality of microbial genomes recovered from isolates, single cells, and metagenomes. *Genome Res* **25**: 1043–1055.
- Peng X, Yu H, Ai L, Li N, Wang X. (2013). Time behavior and capacitance analysis of nano-Fe₃O₄ added microbial fuel cells. *Bioresour Technol* **144**: 689–692.
- Peng Y, Leung HC, Yiu S-M, Chin FY. (2012). IDBA-UD: a de novo assembler for single-cell and metagenomic sequencing data with highly uneven depth. *Bioinformatics* **28**: 1420–1428.
- Pietikäinen J, Kiikkilä O, Fritze H. (2000). Charcoal as a habitat for microbes and its effect on the microbial community of the underlying humus. *Oikos* **89**: 231–242.
- Price MN, Dehal PS, Arkin AP. (2010). FastTree 2—approximately maximum-likelihood trees for large alignments. *PLoS One* **5**: e9490.
- Pruesse E, Peplies J, Glockner FO. (2012). SINA: accurate high-throughput multiple sequence alignment of ribosomal RNA genes. *Bioinformatics* **28**: 1823–1829.
- Quilliam RS, Glanville HC, Wade SC, Jones DL. (2013). Life in the 'charosphere'—Does biochar in agricultural soil provide a significant habitat for microorganisms? *Soil Biol Biochem* **65**: 287–293.
- Rawal A, Joseph SD, Hook JM, Chia CH, Munroe PR, Donne SW et al. (2016). Mineral-biochar composites: molecular structure and porosity. *Environ Sci Technol* **50**: 7706–7714.
- Richardson DJ, Butt JN, Fredrickson JK, Zachara JM, Shi L, Edwards MJ et al. (2012). The 'porin-cytochrome' model for microbe-to-mineral electron transfer. *Mol Microbiol* **85**: 201–212.
- Rondon MR, Goodman RM, Handelsman J. (1999). The Earth's bounty: assessing and accessing soil microbial diversity. *Trends Biotechnol* **17**: 403–409.
- Schmieder R, Edwards R. (2011). Quality control and preprocessing of metagenomic datasets. *Bioinformatics* **27**: 863–864.
- Sessitsch A, Weilharter A, Gerzabek MH, Kirchmann H, Kandeler E. (2001). Microbial population structures in soil particle size fractions of a long-term fertilizer field experiment. *Appl Environ Microbiol* **67**: 4215–4224.
- Singer E, Emerson D, Webb EA, Barco RA, Kuenen JG, Nelson WC et al. (2011a). *Mariprofundus ferrooxydans* PV-1 the first genome of a marine Fe (II) oxidizing Zetaproteobacterium. *PLoS One* **6**: e25386.
- Singer E, Webb EA, Nelson WC, Heidelberg JF, Ivanova N, Pati A et al. (2011b). Genomic potential of *Marinobacter aquaeolei*, a biogeochemical 'opportunistroph'. *Appl Environ Microbiol* **77**: 2763–2771.
- Singer E, Heidelberg JF, Dhillon A, Edwards KJ. (2013). Metagenomic insights into the dominant Fe (II) oxidizing Zetaproteobacteria from an iron mat at Lo'ihi, Hawai'i. *Front Microbiol* **4**: 52.
- Sun D, Meng J, Xu EG, Chen W. (2016). Microbial community structure and predicted bacterial metabolic functions in biochar pellets aged in soil after 34 months. *Appl Soil Ecol* **100**: 135–143.
- Sun Y, Wei J, Liang P, Huang X. (2012). Microbial community analysis in biocathode microbial fuel cells packed with different materials. *AMB Express* **2**: 21.
- Tabita FR, Satagopan S, Hanson TE, Kreel NE, Scott SS. (2008). Distinct form I, II, III, and IV Rubisco proteins from the three kingdoms of life provide clues about Rubisco evolution and structure/function relationships. *J Exp Bot* **59**: 1515–1524.
- Trüper HG. (1994). Reverse siroheme sulfite reductase from *Thiobacillus denitrificans*. *Methods Enzymol* **243**: 422–426.
- Waite JL. (2012). *Characterization of Cytochrome c Peroxidase of Marinobacter Aquaeolei*. Los Angeles, California: University of Southern California.
- Wang Z, Leary DH, Malanoski AP, Li RW, Hervey WJ, Eddie BJ et al. (2015). A previously uncharacterized,

- nonphotosynthetic member of the Chromatiaceae is the primary CO₂-fixing constituent in a self-regenerating biocathode. *Appl Environ Microbiol* **81**: 699–712.
- Wang J, Xiong Z, Kuzyakov Y. (2016). Biochar stability in soil: meta-analysis of decomposition and priming effects. *GCB Bioenergy* **8**: 512–523.
- Westram R, Bader K, Prüsse E, Kumar Y, Meier H, Glöckner FO *et al.* (2011). ARB: a software environment for sequence data. In: de Bruijn FJ (ed.) *Handbook of Molecular Microbial Ecology I*. Hoboken, NJ: John Wiley & Sons, Inc., 399–406.
- Woolf D, Amonette JE, Street-Perrott FA, Lehmann J, Joseph S. (2010). Sustainable biochar to mitigate global climate change. *Nat Commun* **1**: 56.
- Xia X, Sun Y, Liang P, Huang X. (2012). Long-term effect of set potential on biocathodes in microbial fuel cells: electrochemical and phylogenetic characterization. *Bioresour Technol* **120**: 26–33.
- Yariv S, Cross H. (2001). *Organo-Clay Complexes and Interactions*. Taylor & Francis: New York.
- Ye J, Nielsen S, Joseph S, Thomas T. (2015). High-resolution and specific detection of bacteria on complex surfaces using nanoparticle probes and electron microscopy. *PLoS One* **10**: e0126404.
- Ye J, Zhang R, Nielsen S, Joseph SD, Huang D, Thomas T. (2016). A combination of biochar-mineral complexes and compost improves soil bacterial processes, soil quality and plant properties. *Front Microbiol* **7**: 372.
- Yeates TO, Kerfeld CA, Heinhorst S, Cannon GC, Shively JM. (2008). Protein-based organelles in bacteria: carboxysomes and related microcompartments. *Nat Rev Microbiol* **6**: 681–691.
- Yin Y, Huang G, Tong Y, Liu Y, Zhang L. (2013). Electricity production and electrochemical impedance modeling of microbial fuel cells under static magnetic field. *J Power Sources* **237**: 58–63.
- Yu L, Yuan Y, Tang J, Wang Y, Zhou S. (2015). Biochar as an electron shuttle for reductive dechlorination of pentachlorophenol by *Geobacter sulfurreducens*. *Sci Rep* **5**: 16221.

Supplementary Information accompanies this paper on The ISME Journal website (<http://www.nature.com/ismej>)